Single-layer metallodielectric nanostructures as dual-band midinfrared filters

Yan Tang, Jeremy A. Bossard, Douglas H. Werner, and Theresa S. Mayer[a)]
Department of Electrical Engineering, Center for Nanoscale Science, The Pennsylvania State University, University Park, Pennsylvania 16802, USA

(Received 16 March 2008; accepted 12 May 2008; published online 2 July 2008)

We report a design and fabrication strategy for creating single-layer metallodielectric nanostructures with dual-band filtering properties at midinfrared wavelengths. Genetic algorithm optimization was used to determine an arrangement of nanometer-scale metal pixels within one unit cell of a two-dimensional periodic array that best satisfied the user-specified filter response and nanofabrication design rule constraints. Infrared transmission and reflection spectra measured on an optimized nanostructure array had two narrow stop bands blueshifted by 0.2 μm from the designed center wavelengths of 3.3 and 4.1 μm, with transmission attenuation greater than −20 dB and reflection attenuation less than −1.5 dB in each band. This strategy provides a practical and efficient approach to design metallodielectric nanostructures needed for photonic device applications as well as for future low-loss refractive index engineered metamaterials. © *2008 American Institute of Physics*. [DOI: 10.1063/1.2944137]

The interaction of light with metallic nanostructures embedded in a dielectric medium gives rise to optical properties that are being exploited to fabricate photonic devices for infrared filters,[1,2] polarizers,[3] nanoresonators,[4] biosensors,[5] surface-enhanced Raman spectroscopy,[6] and to serve as low- and negative index metamaterials.[7–10] For example, planar metallodielectric structures arranged in a doubly periodic array can be designed to have electromagnetic resonances at frequencies that are determined by the unit cell geometry and constituent materials.[11] Thus, the nanostructures can be tailored for high reflection or transmission that is angle and polarization sensitive or insensitive, which gives rise to a wide range of filtering characteristics in the infrared and terahertz. These basic design principles can also be extended to more sophisticated multilayer nanostructures that simultaneously exhibit negative permittivity and permeability, and hence negative refractive index.[8–10]

Metallodielectric infrared filters have been fabricated from three-dimensional lattices of metallic scatterers[12] or from stacks of identical layers containing two-dimensional periodic arrays of metallic elements.[13,14] Mid/near-infrared stop-band filters with in-band transmission attenuation exceeding −10 dB were demonstrated with as few as three unit cells along the direction of light propagation.[9] More recently, other geometries such as self-similar fractals were used to fabricate long-wave infrared stop-band filters with similar strong in-band attention using only a single-layer structure.[15,16] Increased design flexibility has been achieved by implementing feed-forward genetic algorithm (GA) optimization[17] approaches to identify nonintuitive geometries that meet user-defined performance criteria, including stop or pass-band frequencies, attenuation or reflection, angle, and polarization response.[18]

In this letter, we report the experimental realization of a single-layer metallodielectric filter having two narrow stop bands with attenuation greater than −20 dB in the 3.0–5.0 μm midinfrared atmospheric window. The stringent performance requirements of this midinfrared filter were met by incorporating practical fabrication design rule constraints and the measured dielectric dispersion properties of the constituent materials in the GA optimization of the nanometer-scale unit cell geometry. The strong agreement that was achieved between the experimentally measured filter properties and the modeled response shows that this technique can be scaled for direct nanofabrication of midinfrared metallodielectric photonic devices.

The dual-band midinfrared metallodielectric filter we designed consists of a doubly periodic array of planar metallic nanostructures sandwiched between thin dielectric substrate and superstrate layers, as shown in Fig. 1. The iterative GA design optimization process was conducted by dividing a square unit cell into an 16×16 grid of pixels, and assigning a binary value that indicates the presence ("1") or absence ("0") of metal on the pixel. The scattering parameters of each candidate design were analyzed using a full-wave periodic method of moments (PMoM) electromagnetic modeling code, and then evaluated against an ideal filter response to determine its cost. The cost function used in this work was defined as

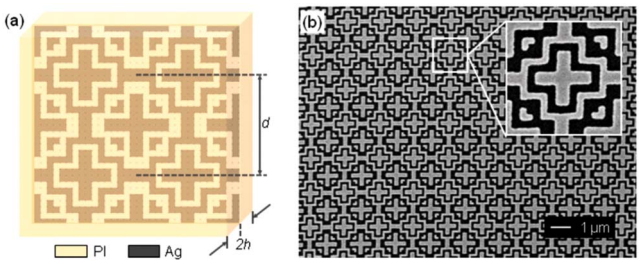

FIG. 1. (Color online) (a) Schematic of the FSS filter optimized by a GA to exhibit dual stop bands at 3.3 and 4.1 μm. The period d of the unit cell is 1.87 μm. The thickness h of the polyimide dielectric layers is 1.07 μm on each side of the silver metal elements. (b) SEM image of a fabricated filter without the top polyimide dielectric layer. The inset shows an enlarged image of one unit cell. The bright areas are the silver elements and the dark areas are the dielectric.

[a)]Electronic mail: tsm2@psu.edu.

$$\text{Cost} = \frac{1}{N_{\text{pass}} N_{\text{pass}}} \sum [\text{MIN}(|T|,0.95) - 0.95]^2 + \frac{1.5}{N_{\text{stop}} N_{\text{stop}}} \sum [\text{MAX}(|T|,0.1) - 0.1]^2,$$

where N_{pass} and N_{stop} are the number of pass and stop-band frequencies, respectively, and T is the transmittance. The ideal filter response was represented as $|T| \geqslant 0.95$ (−0.2 dB) in the pass bands and $|T| \leqslant 0.1$ (−10 dB) in the stop bands. The GA optimization process minimized this cost function and converged to a solution that maximized pass-band transmittance and minimized stop-band transmittance. The GA optimization parameters used for this filter design were the unit cell size, unit cell geometry (i.e., arrangement of metal and dielectric pixels), and thickness of the dielectric layers. Additional fabrication design rules that prohibited corner-to-corner connections between metal elements and maintained a minimum pixel size were applied to enforce geometric constraints required for nanofabrication.

The constituent metal and dielectric materials were silver and polyimide. Silver was used because it has one of the lowest absorption losses in the near to midinfrared frequency regime.[19] The thickness of the silver used in the fabricated structure was 75 nm, which is several times the skin depth in the midinfrared. A thin freestanding polyimide film was applied on each side of the metallic screen to support the metal elements and to protect them from oxidation. Polyimide was selected over other candidate low-loss dielectric materials because of its superior mechanical flexibility and thermal stability, which makes it attractive for many coating applications. The wavelength-dependent dispersive material properties including a published metallic loss model for silver at optical and IR wavelengths[19] and the measured dielectric constant for polyimide were incorporated into the PMoM code.

An example of a metallodielectric nanostructure designed to have two midinfrared stop bands at 3.3 and 4.1 μm and pass bands at all other wavelengths between 2.0 and 6.0 μm for near normal incidence is shown in Fig. 1(a). An eightfold symmetry was imposed on the unit cell geometry to achieve polarization independence. The optimized unit cell dimensions were 1.87×1.87 μm^2 and the thickness of both polyimide dielectric layers was 1.07 μm. The predicted transmission and reflection response of this filter to an unpolarized plane wave at normal incidence are plotted as a function of wavelength in Fig. 2 (red symbols). Both stop bands had transmission attenuation greater than −23 dB and a corresponding loss in reflection intensity lower than −1.5 dB. In the pass bands, the maximum transmission intensity was approximately −0.5 dB, which is primarily due to the impedance mismatch between air and polyimide. These characteristics indicate that this filter operates through reflection and not absorption, which is favorable for maintaining the long-term stability of the devices.

To validate this design and modeling, we fabricated the metallodielectric filter using electron-beam lithography. The process began by spinning a layer of polyimide precursor (diluted HD Microsystem PI2574 resin) onto a sacrificial silicon handle wafer, which was coated on both sides with a 500 nm thick layer of silicon dioxide. The precursor was thermally cured to form an imidized layer in a nitrogen-purged convection oven at 150 °C for 30 min and then at 250 °C for 2 h. A single layer of positive electron-beam resist (3% polymethyl methacrylate 950 K in anisole) was applied to the polyimide substrate and covered with a 10 nm thick layer of conducting gold. Direct write electron-beam lithography (Leica EBPG-5HR) was then used to define a doubly periodic array of the unit cells (1600×1600) in the resist using a dose of 700 μC/cm^2. The resist was developed in a 1:3 solution of methyl-isobutyl-ketone in isopropanol. A 75 nm thick thermally evaporated silver film was lifted-off (Microposit 1165 remover) to leave the silver elements on the polyimide substrate. The process was completed by spin coating and curing the top polyimide layer using the previously described conditions. The film was released from the handle wafer with diluted buffered oxide etchant and mounted onto an aluminum frame for optical characterization. The final metallodielectric filter measured 3 mm on each side and was 2.1 μm thick.

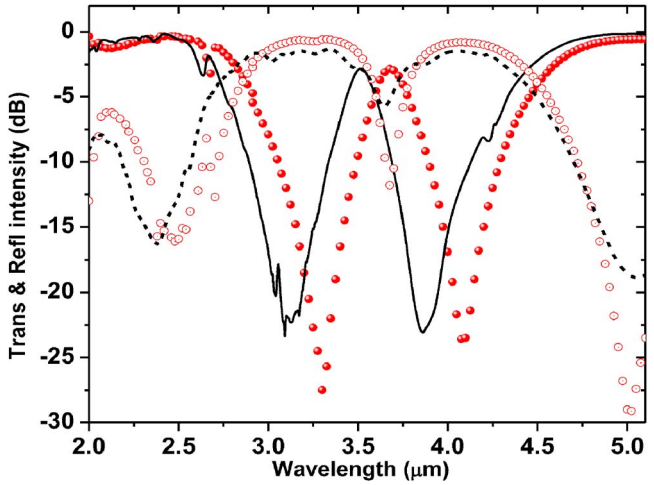

FIG. 2. (Color online) PMoM-modeled transmission spectrum (filled red circles) and reflection spectrum (empty red circles) at normal incidence of the designed metallodielectric filter shown in Fig. 1(a). Measured transmission spectrum at normal incidence (solid black line) and reflection spectrum at 15° (dashed black line) of the fabricated filter. Both spectra were taken using an unpolarized source.

A field-emission scanning electron microscope image of the fabricated metallodielectric filter taken on a sample prior to casting the topmost polyimide superstrate layer is shown in Fig. 1(b). The as-fabricated structure faithfully replicated the unit cell geometry and was uniform across the entire 3×3 mm^2 active area. This was achieved by optimizing the size of the nanometer-scale metal features and the exposure dose to compensate for the proximity effects during electron-beam lithography, which were otherwise found to increase the size of the metal pixels.

The optical response of the metallodielectric filter was characterized using a Fourier transform infrared (FTIR) spectrometer (Bruker Optics model IFS-66) equipped with a silicon carbide Globar™ source, a germanium–potassium bromide beam splitter, and a liquid nitrogen cooled mercury cadmium telluride detector. The sample was placed in a nitrogen-purged compartment and the light from the Globar source was focused onto the sample with a spot size of ~5 mm in diameter and an angular spread of ~6° from the beam direction. The angle of incidence (angle between the sample surface normal and the optical axis) was 0° for the transmission and 15° for the reflection measurement.

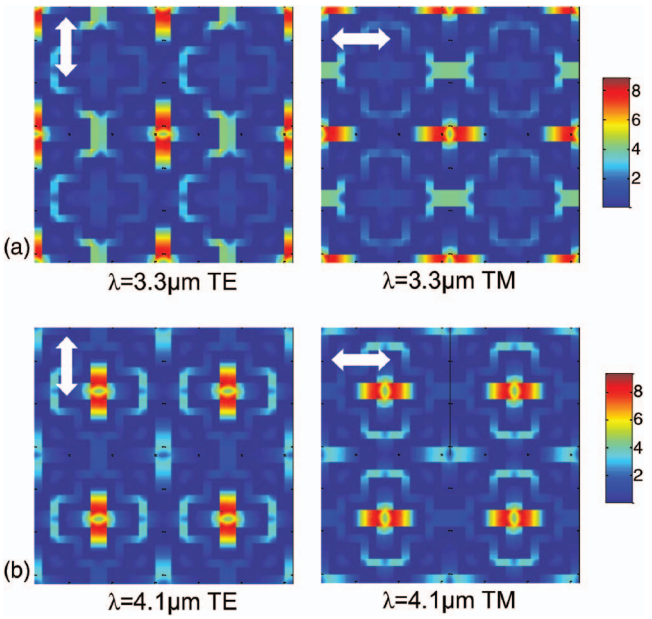

FIG. 3. (Color) The relative surface current distribution on the metal elements at the two resonance wavelengths: (a) 3.3 μm and (b) 4.1 μm for two orthogonal polarizations, induced at normal incidence. The white arrows indicate the polarization. The colored bars indicate the relative current density.

The measured transmission and reflection intensity spectra of the metallodielectric filter are shown as solid and dashed black lines in Fig. 2. The filter response agrees well with the modeled results in terms of the band positions, attenuation/reflection intensities, and bandwidth. Specifically, the transmission spectrum contained two stop bands centered at 3.1 and 3.9 μm each having an attenuation of ~ -22 dB. The peaks in the reflection spectrum were at 3.3 and 4.1 μm with a loss of less than -1.5 dB in each band. The transmission and reflection spectra were both blueshifted by ~ 0.2 μm in comparison to their modeled response, and the attenuation was slightly lower (~ -22 measured compared to -27 and -25 dB modeled). The bandwidths of the transmission stop bands determined from their -3 dB attenuation points were 0.22 and 0.26 μm, as compared to the designed values of 0.19 and 0.24 μm. The small blueshift and increase in bandwidth were due, at least in part, to rounding at the corners of the silver pixels during electron-beam patterning. In addition, as discussed in the experimental methods, the metallodielectric filter was characterized with a focused beam in the FTIR rather than a plane wave as used in the model. This may also account for the lower attenuation and broadening in the transmission stop bands relative to the model. These results demonstrate that this design optimization process can be applied to design midinfrared metallodielectric photonic devices that meet user-input-defined performance criteria using only a single layer of metallic elements.

The physical operating mechanism of this metallodielectric filter was analyzed by investigating the electric current distribution on the metal elements as determined by PMoM modeling. A careful inspection of the current distribution shown in Fig. 3 reveals that two sets of crossed dipoles that are 0.93 and 1.18 μm long are resonant at wavelengths of 3.3 and 4.1 μm, respectively. The surface currents are induced by the incident electromagnetic wave and resonantly enhanced on the dipole elements that have lengths equal to approximately one half of the wavelength in the polyimide dielectric ($\varepsilon_r \approx 2.7$). The presence of this surface current gives rise to a specularly reflected wave with low reflection loss and a 180° phase shift relative to the incident wave at the resonant wavelengths.

In conclusion, we designed and fabricated a metallodielectric filter having two stop bands in the 3.0–5.0 μm midinfrared atmospheric window. The filter is comprised of a doubly periodic array of metal elements sandwiched between two thin dielectric layers with a unit cell geometry that is determined by GA optimization to meet a user-input defined cost function. The transmission spectrum measured at normal incidence had stop bands centered at 3.1 and 4.1 μm, both with attenuation greater than -22 dB and narrow bandwidth of ~ 0.3 μm. The peaks in the reflection spectrum had less than -1.5 dB loss in both bands. The measured response of the filter agreed well with spectra modeled using the PMoM, and validates this GA-based design approach. The flexibility provided by this approach will enable customized design of future metallodielectric photonic devices and allow the balancing of effective medium parameters in refractive-index-engineered nanostructures where small differences in geometry or constituent material properties can greatly impact the medium's effective optical constants.

This work was supported by the Penn State Materials Research Institute and the Penn State MRSEC under NSF Grant No. DMR 0213623. The authors would like to thank J. A. Woollam for variable angle infrared spectroscopic ellipsometry measurements of the polyimide dielectric thin films. The metallodielectric nanostructures were fabricated at the PSU Site of the NSF NNIN under Agreement No. 0335765.

[1] T. W. Ebbesen, H. J. Lezec, H. F. Ghaemi, T. Thio, and P. A. Wolff, Nature (London) **391**, 667 (1998).
[2] Q. Xu, J. Bao, R. M. Rioux, R. Perez-Castillejos, F. Capasso, and G. M. Whitesides, Nano Lett. **7**, 2800 (2007).
[3] Z. Yu, P. Deshpande, W. Wu, J. Wang, and S. Y. Chou, Appl. Phys. Lett. **77**, 927 (2000).
[4] C. E. Hofmann, E. J. R. Vesseur, L. A. Sweatlock, H. J. Lezec, F. J. García de Abajo, A. Polman, and H. A. Atwater, Nano Lett. **7**, 3612 (2007).
[5] A. J. Haes, L. Chang, W. L. Klein, and R. P. Van Duyne, J. Am. Chem. Soc. **127**, 2264 (2005).
[6] A. V. Whitney, J. W. Elam, P. C. Stair, and R. P. Van Duyne, J. Phys. Chem. C **111**, 16827 (2007).
[7] D.-H. Kwon and D. H. Werner, Opt. Express **15** 9267 (2007).
[8] V. M. Shalaev, Nat. Photonics **1**, 41 (2007).
[9] V. M. Shalaev, W. Cai, U. K. Chettiar, H.-K. Yuan, A. K. Sarychev, V. P. Drachev, and A. V. Kildishev, Opt. Lett. **30**, 3356 (2005).
[10] S. Zhang, W. Fan, N. C. Panoiu, K. J. Malloy, R. M. Osgood, and S. R. J. Brueck, Phys. Rev. Lett. **95**, 137404 (2005).
[11] I. Puscasu, D. Spencer, and G. Boreman, Appl. Opt. **39**, 1570 (2000).
[12] K. A. McIntosh, L. J. Mahoney, K. M. Molvar, O. B. McMahon, S. Verghese, M. Rothschild, and E. R. Brown, Appl. Phys. Lett. **70**, 2937 (1997).
[13] J. A. Oswald, B.-I. Wu, K. A. McIntosh, L. J. Mahoney, and S. Verghese, Appl. Phys. Lett. **77**, 2098 (2000).
[14] H. A. Smith, M. Rebbert, and O. Sternberg, Appl. Phys. Lett. **82**, 3605 (2003).
[15] R. P. Drupp, J. A. Bossard, Y. Ye, D. H. Werner, and T. S. Mayer, Appl. Phys. Lett. **85**, 1835 (2004).
[16] R. P. Drupp, J. A. Bossard, D. H. Werner, and T. S. Mayer, Appl. Phys. Lett. **86**, 081 102 (2005).
[17] R. L. Haupt and D. H. Werner, *Genetic Algorithms in Electromagnetics* (Wiley, Hoboken, NJ, 2007).
[18] J. A. Bossard, D. H. Werner, T. S. Mayer, J. A. Smith, Y. Tang, R. P. Drupp, and L. Li, IEEE Trans. Antennas Propag. **54**, 1265 (2006).
[19] A. D. Rakić, A. B. Djurřisic, J. M. Elazar, and M. L. Majewski, Appl. Opt. **37**, 5271 (1998).